Journal of ELECTRONIC MATERIALS, Vol. 48, No. 11, 2019
https://doi.org/10.1007/s11664-019-07533-8
© 2019 The Minerals, Metals & Materials Society

Room Temperature Synthesis of Transparent and Conducting Indium Tin Oxide Films with High Mobility and Figure of Merit by RF-Magnetron Sputtering

AJINKYA BHORDE,[1] RAVINDRA WAYKAR,[1] SHRUTHI NAIR,[1] HARIBHAU BORATE,[1] SUBHASH PANDHARKAR,[1] RAHUL AHER,[1] ASHISH WAGHMARE,[1] PRITI VAIRALE,[1] DHIRSING NAIK,[1] and SANDESH JADKAR[2,3]

1.—School of Energy Studies, Savitribai Phule Pune University, Pune 411 007, India. 2.—Department of Physics, Savitribai Phule Pune University, Pune 411 007, India. 3.—e-mail: sandesh@physics.unipune.ac.in

Tin doped indium oxide (ITO) films with high conductivity and charge carrier mobility were deposited at room temperature using RF-magnetron sputtering, without any post annealing treatment. It is observed that structural, optical, morphological and electrical properties of these ITO films depend on deposition time. All the synthesized films show optical transmittance $> 90\%$ and band gap of ~ 3.6 eV. A change in crystal orientation from (222) to (400) with slight shift of peaks toward lower 2θ has been observed with the increase in deposition time. The synthesized films are compact, uniform and free from cracks. Moreover, there was an increase in grain size and shape with the progress in deposition time. Synthesized ITO films with (400) orientation have high conductivity ($\sim 2 \times 10^3\ \Omega^{-1}\ \mathrm{cm}^{-1}$), high charge carrier mobility ($\sim 348\ \mathrm{cm}^2\ \mathrm{V}^{-1}\ \mathrm{s}^{-1}$) and a high figure of merit ($104 \times 10^{-3}\ \Omega^{-1}$). The synthesized thin films can have prospective applications in opto-electronic devices such as solar cells, light emitting diodes, etc.

Key words: Indium tin oxide (ITO), sputtering, structural properties, optical properties, figure of merit

INTRODUCTION

Transparent conducting oxides (TCOs) such as doped ZnO, In_2O_3, SnO_2 etc., play a significant role as transparent electrodes in various opto-electronic devices. The existence of transparency and electrical conductivity are normally contradictory to each other but TCOs possess both of these properties simultaneously. TCOs are generally n-type wide band gap semiconductors (*p*-type too) with a relatively high concentration of free electrons in the conduction band. The wide band gap is responsible for high optical transmittance whereas large number of free electrons are responsible for high electrical conductivity. Indium tin oxide (ITO) thin films as TCO layer has attracted a lot of interest in recent years due to high optical transparency in the visible and near-infrared region, high electrical conductivity and an inherent wide band gap > 3.5 eV. ITO has been successfully employed in various opto-electronic devices such as photovoltaic cells,[1] liquid crystal displays[2] and gas sensors.[3]

ITO thin films are commonly synthesized by employing different techniques such as magnetron sputtering,[4] the sol–gel process,[5] thermal evaporation,[6] pulsed laser deposition (PLD),[7] chemical vapour deposition,[8] atomic layer deposition (ALD),[9] spray pyrolysis,[10] jet nebulizer spray pyrolysis,[11] chemical solution deposition (CSD) process,[12] electron beam evaporation method[13] etc. The electrical and optical properties of ITO film strongly depend on its structure, tin content, etc. Each

(Received March 11, 2019; accepted August 7, 2019; published online August 19, 2019)

deposition method has its own merits and demerits and thereby yields films with different properties. For example, PLD method results in TCO coatings with appropriate electrical and optical properties,[14] with its major advantage being preservation of the target chemical composition in the transferred films. However, a major disadvantage associated with the PLD process is, high kinetic energy of laser plume causing re-sputtering which creates defects on the substrate surface and on the growing film.[15] Spray pyrolysis is the most attractive technique for the synthesis of ITO thin films, as the set-up is simple and the process can be scaled up easily.[16] However, it is difficult to control the film thickness and also homogeneity over the substrate area in spray pyrolysis technique.[17] Furthermore, cooling of the substrate during deposition significantly affects the film structure.[18] RF-magnetron sputtering technique has received considerable attention as ITO thin films of desired opto-electronic properties can be easily synthesized. A major advantage of RF-magnetron method is that it results in ITO coatings with desired opto-electronic properties, preserves the target chemical composition and also maintains stoichiometry. Moreover, it allows deposition to occur at low substrate temperature, gives better adhesion, larger coverage, high uniformity, controllable thickness, high surface mobility in condensing particles, conformal films morphologies and dense film compared to other methods.

It is reported in the literature that to obtain ITO films with desired opto-electrical properties, the films are either deposited at high substrate temperature or requires high temperature post annealing treatment. High substrate temperature or high temperature post annealing treatment limits its use in device fabrication. In this paper we report device quality ITO films synthesized at room temperature by RF-magnetron sputtering. The effect of deposition time on the structural, morphological and opto-electrical properties of RF-magnetron sputtered ITO films has been investigated. We observed that these properties critically depend on the deposition time.

EXPERIMENTAL

Film Preparation

The ITO thin films were deposited on Corning #7507 substrates using in-house built RF-magnetron sputtering system details of which have been described elsewhere.[19] It consists of a cylindrical stainless steel chamber coupled with turbo molecular and rotary pumps which yields a base pressure less than 1.33×10^{-7} kPa. An ITO target with a composition of 90% In_2O_3 and 10% SnO_2 having diameter of 4 inch (Vin Karola Instrument, USA) was used for the deposition of ITO films. The target was kept facing the substrate holder at $\sim$ 7 cm away. In order to obtain films of uniform thickness, substrates were kept rotating during the whole sputtering process using a stepper motor with variable speed. The RF power was kept at 120 W and the deposition time was varied between 8 min to 40 min (in steps of 8 min). The substrates can be clamped on a substrate holder which is heated by inbuilt heater controlled using thermocouple and temperature controller. All depositions were carried out at 25°C. The pressure during deposition was kept constant (0.0021 kPa) using an automated throttle valve and was measured with a capacitance manometer. Prior to each deposition, substrates were cleaned using a standard cleaning procedure. The substrate holder and deposition chamber were baked for 2 h at 100°C in vacuum to remove any water vapour absorbed on the substrates and to remove the oxygen contamination from the film. Sputter-etch of 10 min were used to remove the target surface contamination. The deposition was carried out for different durations and then the films were taken out for characterization.

Material Characterization

X-ray diffraction was performed using x-ray diffractometer (Bruker D8 Advance, Germany) having CuKα line (λ = 1.54056 Å) with a range of 2θ values from 20° to 65° (with step of 0.1°). The optical band gap and thickness of ITO films were estimated from the transmittance spectra recorded using a JASCO, V-670 UV-VIS-NIR spectrometer in the range of 300–1200 nm. For the estimation of band gap and film thickness we have followed the method introduced by Tauc[20] and Swanepoel,[21] respectively.The film thickness was also confirmed by surface profiler (KLA Tencor, P-16+). Microscopic features of ITO films were studied using HITACHI, S-4800, Japan field emission scanning electron microscopy (FE-SEM)and non-contact mode atomic force microscopy (NC-AFM) (JEOL, JSPM-5200). The elemental composition of ITO was made using energy dispersive x-ray spectroscopy (EDAX) attached to the FE-SEM instrument. The bulk concentration, resistivity, sheet resistance, electrical conductivity and charge carrier mobility measurements of ITO films were carried by using Hall Effect measurement (Ecopia HMS-3000, Bridge Technology, USA) unit with applied magnetic field of 0.5 Tesla. The *Williamson–Hall* (W–H) method was used for the residual strain calculations.

RESULTS AND DISCUSSION

X-ray Diffraction Analysis

Figure 1 shows the x-ray diffraction (XRD) pattern of ITO films deposited for different deposition time using RF-magnetron sputtering. Presence of multiple peaks indicates polycrystalline nature of ITO films. Major diffraction peaks were observed at $2\theta \sim 21.5°$, 30.5°, 35.4°, 37.6°, 51°, 56° and 60.6° corresponding to (211), (222), (400), (411), (440), (611) and (622) diffraction planes, respectively.

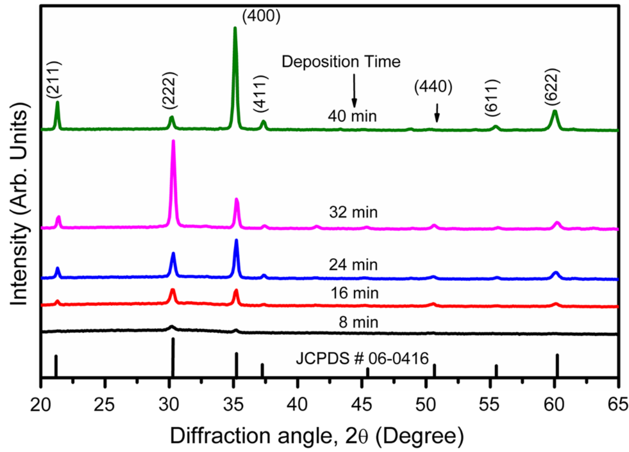

Fig. 1. X-ray diffraction pattern of ITO films deposited using RF-magnetron sputtering for various deposition times.

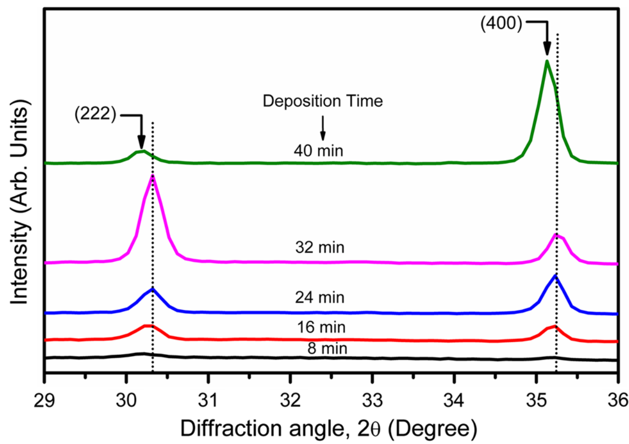

Fig. 2. Magnified x-ray diffraction pattern of ITO films deposited at various deposition time indicating shift of (222) and (400) diffraction planes towards lower 2θ values.

These peak positions are in good agreement with the JCPDS data card # 06-0416 corresponding to the standard XRD pattern of cubic structure of ITO films.[22] As seen from the figure, with increase in deposition time the intensity of (222) and (400) diffraction planes changes significantly. Up to deposition time of 32 min, ITO films shows preferred orientation of crystallites in (222) direction whereas the ITO film deposited for 40 min has preferential orientation in (400) direction. Furthermore, with increase in deposition time from 8 min to 40 min diffraction planes, (222) and (400) shifts towards lower 2θ values (see Fig. 2). These results indicate that ITO films deposited for higher deposition time are under tensile stress.[23] Figure 3 shows the Rietveld refinement for the ITO films deposited for 32 min and 40 min of deposition time. The corresponding estimated parameters are shown in the inset of Fig. 3a and b. The average crystallite size ($d_{\text{x-ray}}$) of ITO films was calculated by the *Scherrer's* formula,[24]

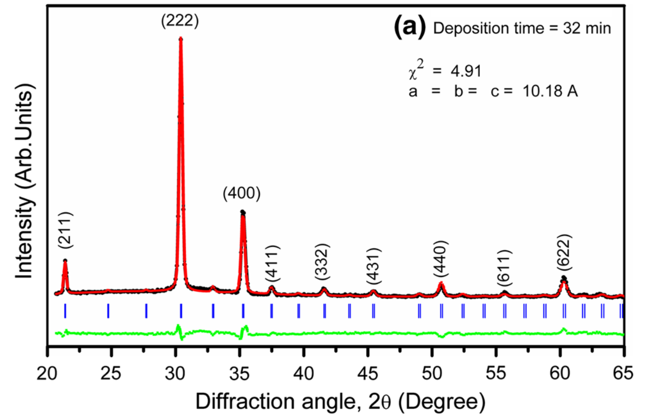

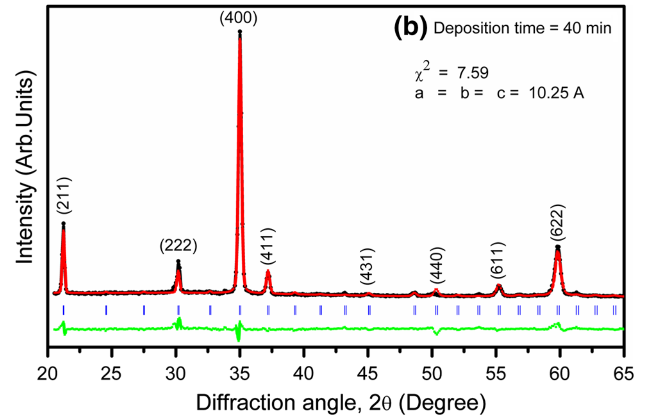

Fig. 3. Rietveld refined x-ray diffraction pattern of RF sputtered ITO films for deposition time 32 min and 40 min. Observed and the calculated profiles are denoted by black and red solid lines, respectively. Positions of the Bragg reflection are shown by short vertical blue markers and the lower curve denotes difference between observed and calculated profiles.

$$d_{\text{x-ray}} = \frac{0.9\lambda}{\beta\cos\theta_B}, \quad (1)$$

where, λ is the wavelength of diffracted radiation, θ_{B} is the Bragg angle and β is the full width at half maximum (FWHM) in radians.

The volume of unit cell (V) of ITO films has been calculated from the equation,

$$V = a^3. \quad (2)$$

The dislocation density (δ) and strain (ϵ) in ITO films deposited for 32 min and 40 min using RF-magnetron sputtering were calculated using following equations,[11]

$$\delta = \frac{1}{d^2_{\text{x-ray}}}, \quad (3)$$

and

$$\varepsilon = \frac{\beta\cos\theta}{4}. \quad (4)$$

The calculated structural parameters of ITO films deposited for 32 min and 40 min deposition time for all (*hkl*) planes are tabulated in Table I. The average crystallite size was found in the range of 19.1 nm to 33.6 nm for ITO films deposited for 32 min of duration and 19.1 nm to 40.4 nm for 40 min of duration. Due to tensile stress a small expansion in the unit cell of ITO has been observed. This was further confirmed from the Rietveld refinement analysis.

The dislocation density was found in the range 8.8×10^{14} lines/m^2 to 27.4×10^{14} lines/m^2 for the ITO films deposited for 32 min of duration and 6.0×10^{14} lines/m^2 to 27.4×10^{14} lines/m^2 for 40 min duration. The values of strain were found in the range of 10.3×10^{-3} to 18.1×10^{-3} for the ITO films deposited for 32 min duration and 0.8×10^{-3} to 18.1×10^{-3} for 40 min of duration. The change in average crystallite size can be attributed to reduction in the dislocation density of corresponding diffraction plane in the ITO films. The dislocation density measures the defects in the crystal structure. These results confirm the improvement in crystalline quality of ITO films with increase in deposition duration. The dislocations, point defects such as site disorder, vacancies, etc., in the crystal structure can introduce lattice strain in the film.[11] The observed reduction in strain is related to the change in shape of the particles and indicates reduction of point defects. The FE-SEM analysis further support this (discussed later).The residual strain induced in the ITO films for deposition duration of 16 min, 24 min, 32 min and 40 min were calculated using the *Williamson–Hall* (W–H) method.[25,26] The breadth of the Bragg peak is a combination of both instrument and sample dependent effects. To decouple this effect it is necessary to collect a diffraction pattern from the line broadening of a standard material such as silicon (to determine instrumental broadening). The instrument-corrected broadening β_D corresponding to diffraction peak of ITO was calculated from following relations,[27]

$$\beta_D^2 = \left[(\beta^2)_{\text{Measured}} - (\beta^2)_{\text{Instrumental}}\right], \tag{5}$$

$$D = \frac{K\lambda}{\beta_D \cos\theta}. \tag{6}$$

Crystal imperfection and distortion due to strain induced broadening is given by $\varepsilon \approx \left(\frac{\beta_s}{\tan\theta}\right)$. Equation 5 has diffraction angle (θ) dependency, whereas the W–H plot method does not have $\left(\frac{1}{\cos\theta}\right)$ dependency and it varies as $\tan(\theta)$. When microstructure causes occurrence of small crystallites size and microstrain together, then θ dependency allow separation of reflection broadening. The size and strain broadening components together contribute to the width of the breadth of a Bragg peak.[28] By considering the Scherer equation and $\varepsilon \approx \left(\frac{\beta_s}{\tan\theta}\right)$ we can write as,

$$\beta_{hkl} = \beta_s + \beta_D, \tag{7}$$

$$\beta_{hkl} = \left(\frac{K\lambda}{\beta_D \cos\theta}\right) + (4\varepsilon \tan\theta). \tag{8}$$

Rearranging Eq. 6 we get,

$$\beta_{hkl} \cos\theta = \left(\frac{K\lambda}{D}\right) + (4\varepsilon \sin\theta). \tag{9}$$

By plotting $\beta_{hkl}\cos\theta$ versus $4\sin\theta$, residual strain of ITO thin films can be extracted from the slope of the fitted line. The W–H plot for all the deposited ITO thin films is shown in Fig. 4. It is interesting to note that the value of crystallite size and strain as estimated from W–H plot matches well with the lattice strain calculations (see Table I).

Optical Properties

Optical transmission and reflection spectrum of RF-magnetron sputtered ITO thin films as a function of deposition time is shown in Fig. 5a in the range of 300–1200 nm. The optical transmission of ITO thin films for different deposition duration times is almost > 90% over the entire range of the

Table I. Crystallite size ($d_{\text{x-ray}}$), dislocation density (δ) and strain (ϵ) for ITO films deposited for 32 and 40 min deposition time

(*hkl*) plane	Deposition time = 32 min			Deposition time = 40 min		
	$d_{\text{x-ray}}$ (nm)	δ ($\times 10^{14}$) (Lines/m^2)	ε ($\times 10^{-3}$)	$d_{\text{x-ray}}$ (nm)	δ ($\times 10^{14}$) (Lines/m^2)	ε ($\times 10^{-3}$)
(211)	33.6	8.8	10.3	40.4	6.0	0.8
(222)	27.4	13.3	12.6	27.4	13.3	12.7
(400)	30.8	10.5	11.2	32.0	9.0	10.8
(411)	25.4	15.5	13.6	27.0	13.7	12.8
(440)	20.9	22.9	16.6	19.9	25.3	17.4
(611)	23.6	18.0	14.7	23.0	18.9	15.1
(622)	19.1	27.4	18.1	19.1	27.4	18.1

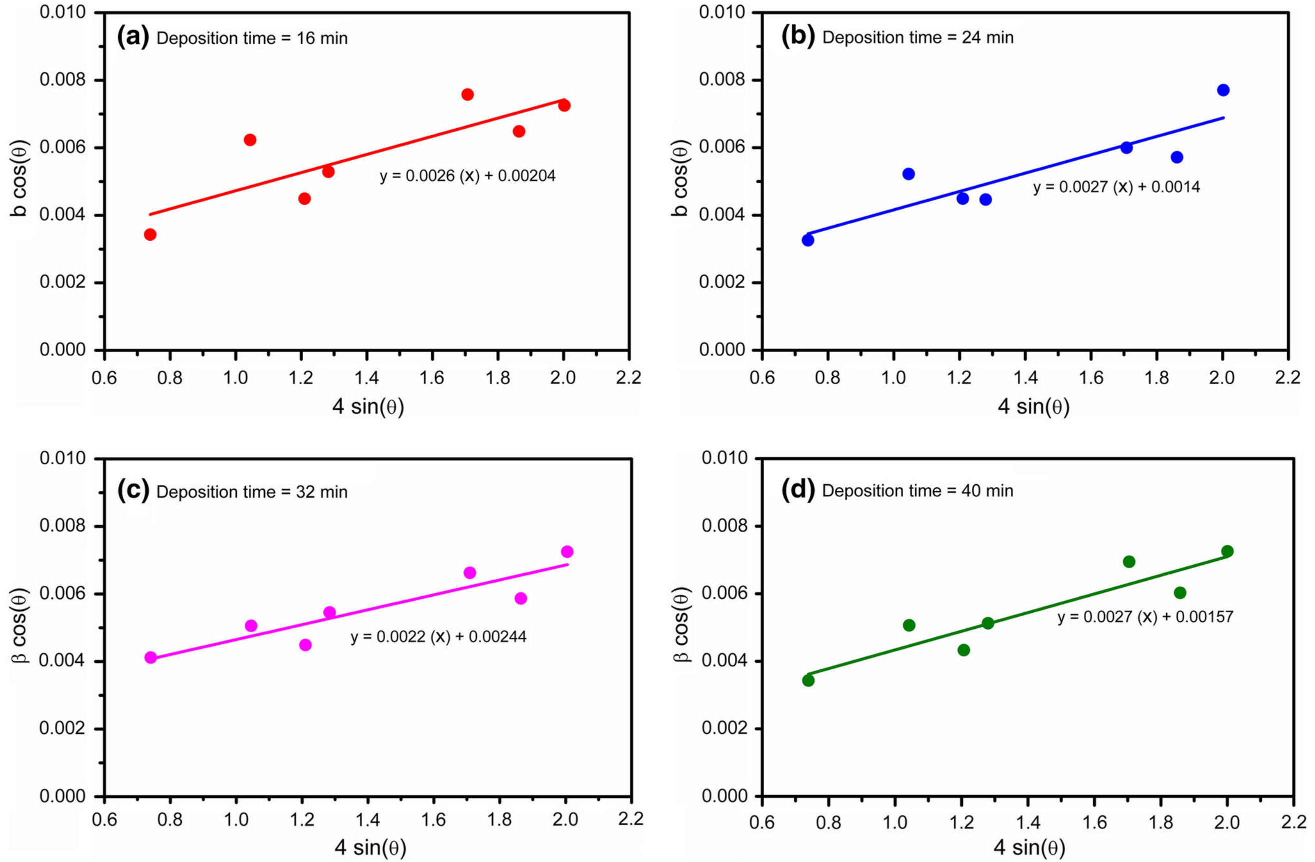

Fig. 4. $\beta_{hkl}\cos\theta$ versus $4\sin\theta$ plots (Williamson–Hall (W–H) plots) for the ITO films deposited for 16 min, 24 min, 32 min and 40 min durations to calculate crystal distortion induced residual strain and crystallite size.

solar spectrum. The optical reflection was found < 15–20% in visible range of the solar spectrum. These results suggest that ITO thin films can have potential applications in opto-electronic devices such as solar cells, as it can reduce the reflection losses. It has been observed that distance between two successive crests and troughs in the interference pattern decreases successively indicating that the thickness of ITO films increases with increase in deposition duration. The thickness of ITO thin films was calculated using method given by Swanepoel[21] and it was found to be 390 nm, 715 nm, 1000 nm, 1329 nm and 1826 nm for deposition duration of 8 min, 16 min, 24 min, 32 min and 40 min, respectively.

The optical band gap of ITO thin films was calculated using Tauc plots[20] through optical transmission and absorption data. The relation between incident photon energy (hν) and absorption coefficient (α) is as follows,

$$(\alpha h\nu)^{1/2} = B^{1/2}(h\nu - E_g), \quad (10)$$

where E_g is band gap energy and B is constant. On extrapolation, the linear portion that cuts the x-axis gives the optical bandgap value. Figure 5b shows the Tauc plots for ITO films deposited for various deposition durations. The band gap values are in the range of 3.6–3.8 eV. The calculated optical band gap values of ITO films matches well with the earlier reports.[29]

Morphology and Surface Properties

Figure 6 shows the FE-SEM micrographs of ITO thin films deposited for various deposition durations. All micrographs were captured at 300,000× magnification. As seen, all synthesized films are dense, compact, and uniform, i.e., without pinholes and cracks. However, a significant change has been observed in the morphology of ITO films deposited for different deposition durations. For the ITO film deposited for 8 min granular grains were observed (Fig. 6a1). The average grain size was found in the range of ~ 20–40 nm. However, the ITO film deposited for 24 min deposition duration shows triangular grains with average size ~ 50–90 nm (Fig. 6a2). The film deposited for 40 min deposition duration also shows triangular grains with increased average size (Fig. 6a3). The average grain size for this film is in the order of 100–160 nm. The increase of grain size may be due to the relaxation of grains for longer deposition durations. The inset of EDAX spectra (Fig. 6b1–b3) gives the quantitative information of elemental mapping of various

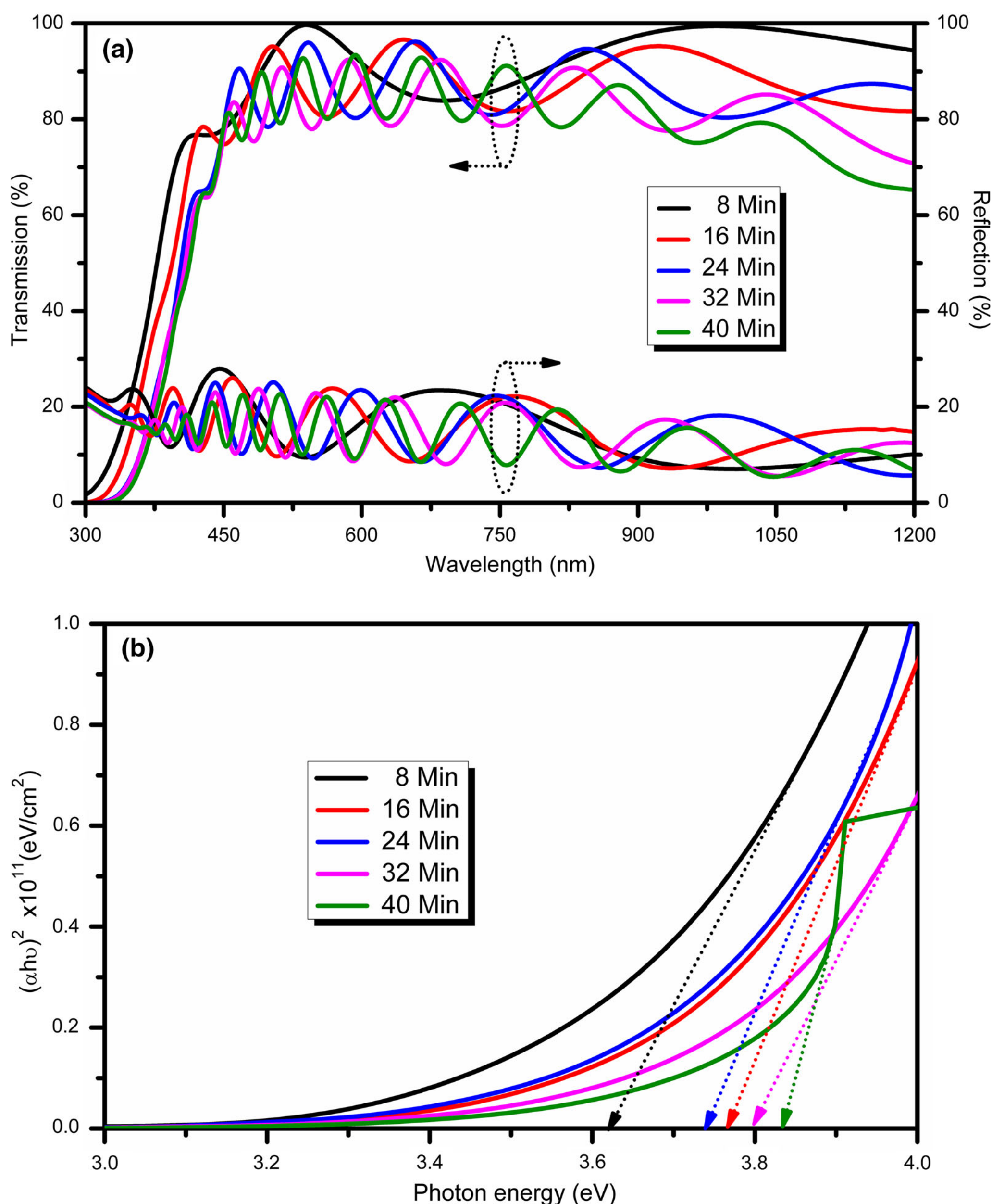

Fig. 5. (a) UV–visible transmission and reflectance spectra of ITO thin films deposited for different deposition time, and (b) combined typical Tauc plot of ITO films deposited for deposition time of 16 min, 24 min, 32 min and 40 min for estimating of band gap.

elements present in the synthesized ITO films. As seen Indium (In) to Tin (Sn) ratio (In/Sn) is found almost constant in all the synthesized samples.

The surface roughness analysis of ITO thin films was carried out by non-contact atomic force microscopy (NC-AFM). The surface features of deposited ITO thin films were studied by measuring root mean square (RMS) roughness values. Figure 7 shows the 3D AFM images of ITO films deposited for different durations. As the deposition time is increased from 8 min to 40 min, the increase in RMS roughness from 1.19 nm to 2.08 nm is clearly observed from Fig. 7. Employment of such ITO films in solar cells can enhance its efficiency by effectively trapping of light due to increase in surface roughness.

Electrical Properties Measurements

Hall Effect measurements were carried out using the *Van der Pauw* method in order to estimate the electrical properties of synthesized thin films. The electrical conductivity, resistivity, Hall mobility, sheet resistance and bulk concentration values were estimated from the advance Ecopia HMS-3000 system. For Hall measurements ITO film of dimension 1 cm $\times$ 1 cm was taken and four indium wire contacts were made at the four corners of the

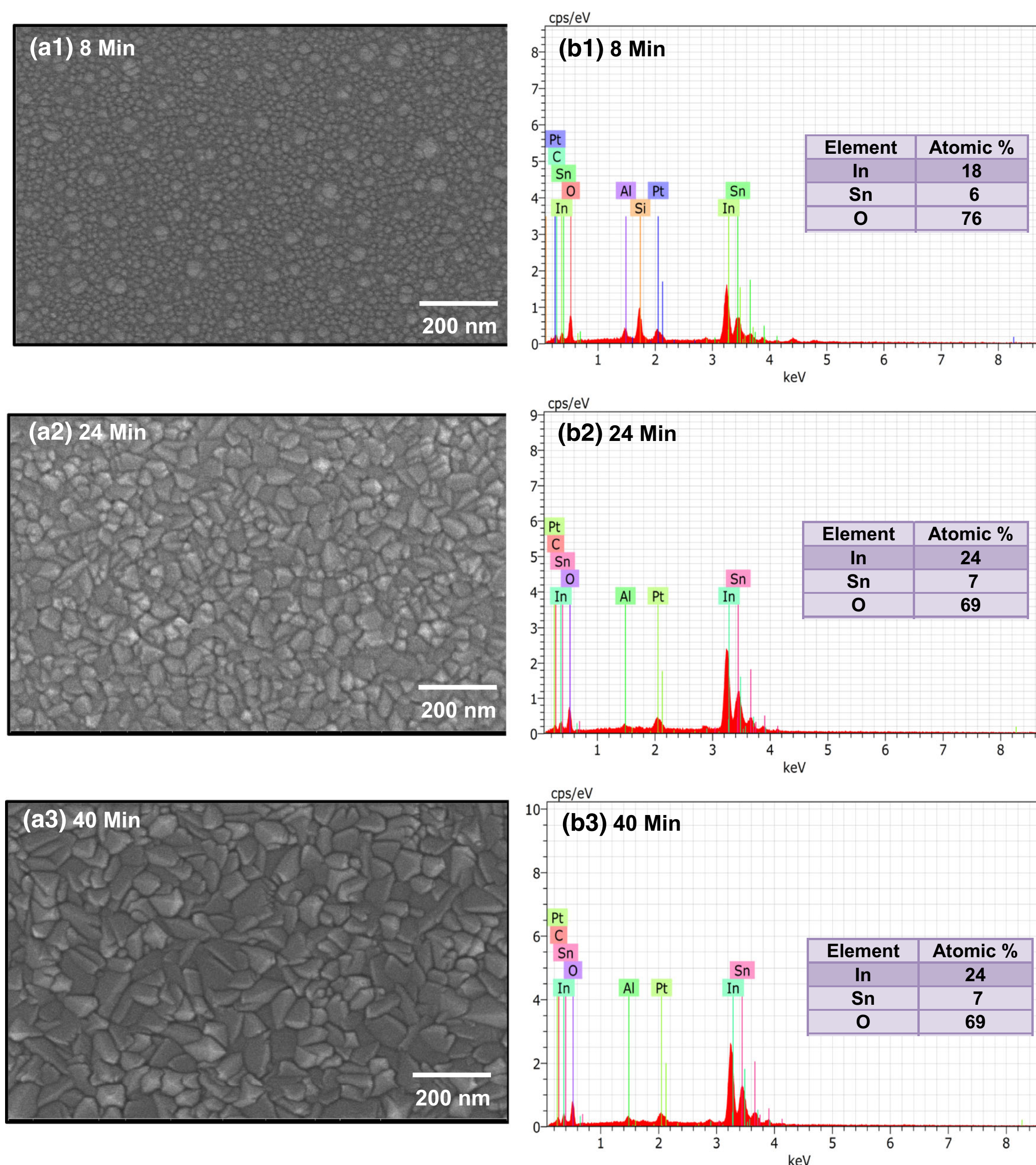

Fig. 6. Field emission scanning electron microscopy (FE-SEM) images of ITO film deposited at (a1) 8 min, (a2) 24 min, (a3) 40 min and EDXA spectra of ITO films deposited for (b1) 8 min, (b2) 24 min, (b3) 40 min.

sample. The current was varied from 1 μA to 10 μA in four steps with an interval of 3 μA. The Hall parameters were recorded during each step by in-built software. The influence of deposition duration on intrinsic properties such as electrical conductivity, resistivity, sheet resistance and charge carrier mobility are shown in Fig. 8. The vertical bars in the figure show the standard mean error occurred in measuring these intrinsic properties. As seen from Fig. 8a the sheet resistance decreases from 22 $\Omega/\square$ to 3 $\Omega/\square$ with increase in deposition time. A low sheet resistance ($\sim$ 3 $\Omega/\square$) was observed for ITO film deposited for 40 min duration. For the same film, the highest conductivity has been observed ($\sim 2 \times 10^3\ \Omega^{-1}\mathrm{cm}^{-1}$). The charge carrier concentration decreases slightly from 3×10^{20} cm^{-3} to 1×10^{20} cm^{-3} when the deposition duration increases from 8 min to 40 min (Fig. 8b). It is interesting to note that the charge carrier mobility increases significantly from 35 cm^2 V^{-1} S^{-1} to 348 cm^2 V^{-1} S^{-1} when deposition time was increased from 8 min to 40 min. The increase in charge carrier mobility can be attributed to change in preferred orientation of ITO crystallites from (222) to (400).

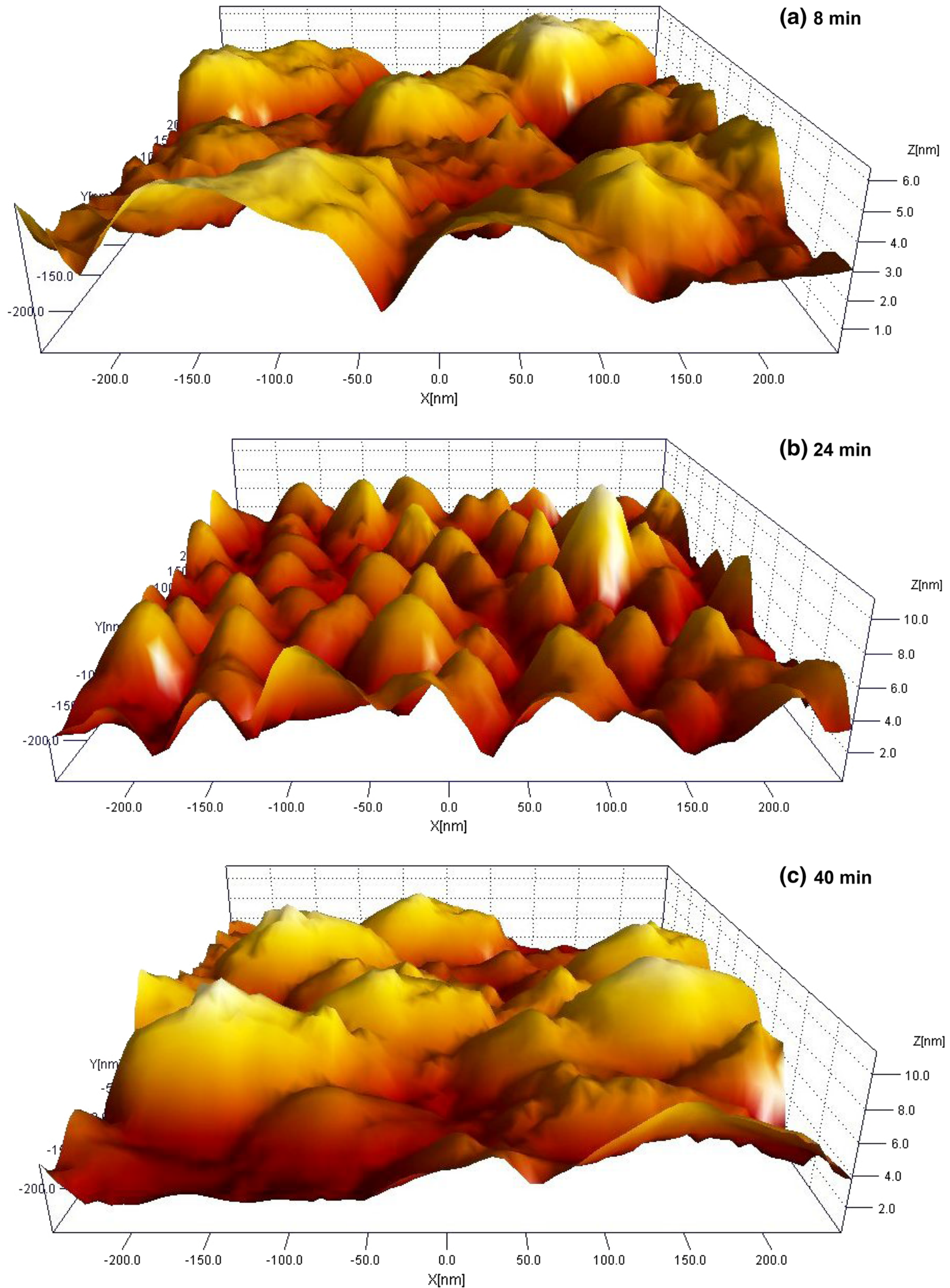

Fig. 7. 3D AFM images for ITO films deposited using RF-magnetron sputtering for different deposition times (a) 8 min, (b) 24 min and (c) 40 min.

Evaluation of ITO as TCO Material

The selection of TCO material requires optimum thickness with good optical and electrical properties. Figure of merit is an important parameter which is used to evaluate the TCO material.[30] The transparent conducting material is well characterized by its electrical sheet resistance (R_{sh}) and optical transmittance (T). The optical transmittance was measured from UV–Visible spectroscopy and

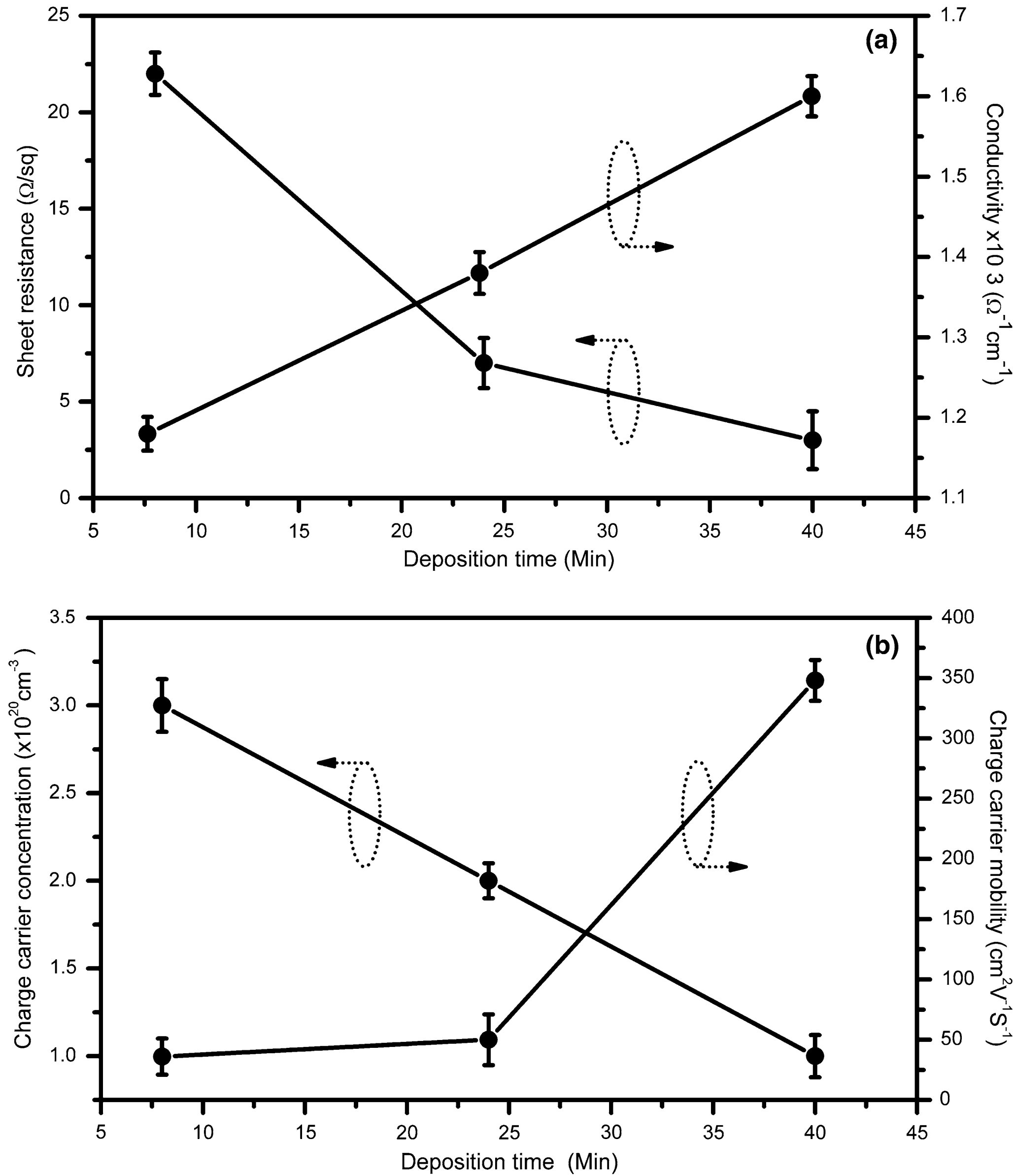

Fig. 8. Hall Effect measurements (a) sheet resistance and electric conductivity and (b) charge carrier concentration and mobility of ITO films as a function of deposition time.

the electrical sheet resistance was estimated from Hall Effect measurement unit. According to Fraser and Cook[31] figure of merit (F_{TC}) is given by,

$$F_{FC} = \frac{T}{R_{sh}}. \tag{11}$$

Here, the expression of figure of merit is inclined towards sheet resistance, so maximum value of figure of merit is obtained for thick film. The figure of merit has been redefined (φ_{TC}) using the following equation, which balances optical transmittance and sheet resistance,[30,32]

$$\phi_{FC} = \frac{T^{10}}{R_{sh}}. \tag{12}$$

Based on the method adapted in Eqs. 11 and 12 figure of merit for synthesized ITO films deposited for different deposition duration is listed in Table II.

As evident from Table II, the ITO film deposited for a duration of 40 min has maximum figure of merit (Both φ_{TC} = 104 × 10^{-3} Ω^{-1} and F_{TC} = 296 × 10^{-3} Ω^{-1}) with high optical transparency (~ 89%) and conductivity (2 × 10^3 Ω^{-1} cm^{-1}). Thus, the ITO films obtained by RF-magnetron sputtering of

Table II. Values of thickness (t), transmission (T), sheet resistance (R_{sh}), figure of merits (F_{TC} and φ_{TC}) at various deposition times

Deposition time (min)	t (nm)	T (at 550 nm)	R_{sh} (Ω/□)	T^{10}	F_{TC} (10^{-3} Ω^{-1})	φ_{TC} (10^{-3} Ω^{-1})
8	390	0.98	22	0.81	44	36
24	715	0.97	7	0.73	138	104
40	1000	0.89	3	0.31	296	104

40 min duration can have potential applications in thin film solar cells and LEDs.

CONCLUSION

In summary, we have deposited tin doped indium oxide (ITO) films using RF-magnetron sputtering at room temperature. The structural, optical, morphological and electrical properties of these films were investigated as a function of deposition time, where other deposition parameters were kept constant. From XRD analysis it has been observed that with increase in deposition time the preferred crystal orientation of ITO crystallites changes from (222) to (400) with slight shift of diffraction peak towards lower diffraction angles due to tensile stress. The optical properties shows the transmittance $> 90\%$ and the bandgap ~ 3.6 eV for all synthesized samples. FE-SEM analysis reveal the formation of compact, uniform, crack-free thin film with increase in average grain size with deposition duration. The (400) oriented film shows improved electrical properties with high mobility (~ 348 cm^2 V^{-1} s^{-1}), minimum sheet resistance (~ 3 Ω/□) and high electrical conductivity (2×10^3 Ω^{-1} cm^{-1}) together with charge carrier concentration $\sim 10^{20}$ cm^{-3}. The figure of merit (φ_{TC}) was also found at a maximum (104×10^{-3} Ω^{-1}) for (400) oriented ITO thin film.

From these results, we can conclude that the synthesized ITO thin films are suitable for optoelectronic applications. Moreover, RF-magnetron sputtering is capable of producing uniform, device quality films at room temperature and that too without any post annealing treatment.

ACKNOWLEDGMENT

Ajinkya Bhorde is thankful to the Department of Science and Technology (DST), Government of India for INSPIRE fellowship. Ravindra Waykar, Shruthi Nair, Subhash Pandharkar, Ashish Waghmare and Dhirsing Naik are thankful to the Ministry of New and Renewable Energy (MNRE), Government of India for the financial support under the National Renewable Energy Fellowship (NREF) program. Rahul Aher is thankful to Savitribai Phule Pune University, Pune for the award of Bharatratna J. R. D. Tata Gunwant Sanshodhak Shishyavruti. All authors are thankful to the Central Instrumentation Facility (CIF), Savitribai Phule Pune University for providing analytical facilities. One of the authors, Sandesh Jadkar, is thankful to the University Grants Commission (UPE program), New Delhi and the Indo-French Centre for the Promotion of Advanced Research-CEFIPRA, Department of Science and Technology, New Delhi for special financial support.

REFERENCES

1. G. Liang, Y. Luo, J. Hu, X. Chen, Y. Zeng, Z. Su, J. Luo, and P. Fan, *Surf. Coat. Technol.* 358, 762 (2019).
2. Y. Liu, J. Sun, H. Liu, and D. Seo, *Liq. Cryst.* (2018). https://doi.org/10.1080/02678292.2018.1554770.
3. M. Abdullah, M. Mamat, A. Ismail, M. Malek, A. Suriani, M. Ahmad, I. Banu, R. Amiruddin, and M. Rusop, *Mater. Lett.* 236, 460 (2019).
4. B. Sahu, W. Long, and J. Han, *ScriptaMaterialia* 149, 98 (2018).
5. M. Misra, D. Hwang, Y. Kim, J. Myoung, and T. Lee, *Ceram. Int.* 44, 2927 (2018).
6. K. Pan, L. Lin, L. Chang, and H. Shih, *Appl. Surf. Sci.* 273, 12 (2013).
7. M. Socol, N. Preda, O. Rasoga, A. Costas, A. Stanculescu, C. Breazu, F. Gherendi, and G. Socol, *Coatings* 9, 19 (2019).
8. H. Nishinaka and M. Yoshimoto, *Cryst. Growth Des.* 18, 4022 (2018).
9. H. Salami, A. Uy, A. Vadapalli, C. Grob, V. Dwivedi, and R. Adomaitis, *J. Vac. Sci. Technol. A* 37, 010905 (2019).
10. V. Brinzari, I. Damaskin, L. Trakhtenberg, B.K. Cho, and G. Korotcenkov, *Thin Solid Films* 552, 225 (2014).
11. M. Thirumoorthia and J. Thomas Joseph Prakash, *J. Asian Ceram. Soc.* 4, 124 (2016).
12. M. Tsai, C. Wang, and M. Hon, *Surf. Coat. Technol.* 172, 95 (2003).
13. H. Kobayashi, T. Ishida, K. Nakamura, Y. Nakato, and H. Tsubomura, *J. Appl. Phys.* 72, 5288 (1992).
14. R. Eason, *Pulsed Laser Deposition of Thin Films* (Hoboken: Wiley, 2007), p. 240.
15. P.R. Willmott and J.R. Huber, *Rev. Mod. Phys.* 72, 315 (2000).
16. P.S. Patil, *Mater. Chem. Phys.* 59, 185 (1999).
17. M. Fujimoto, T. Urano, S. Murai, and Y. Nishi, *Jpn. J. Appl. Phys.* 28, 2587 (1989).
18. G. Korotcenkov and B.K. Cho, *Prog. Cryst. Growth Charact. Mater.* 63, 1 (2017).
19. A. Jadhavar, A. Bhorde, V. Waman, A. Funde, A. Pawbake, R. Waykar, D. Patil, and S. Jadkar, *Eng. Sci. Int. Res. J.* 3, 126 (2015).
20. J. Tauc, *Mater. Res. Bull.* 3, 37–46 (1968).
21. R. Swanepoel, *J. Phys. E* 16, 1214 (1983).
22. F. Gu, R. Nie, Z. Tian, D. Han, and Z. Wang, *RSC Adv.* 5, 99018 (2015).
23. M.K. Trivedi, R.M. Tallapragada, A. Branton, D. Trivedi, G. Nayak, O. Latiyal, and S. Jana, *Ind. Eng. Manag.* 4, 1000177 (2015).
24. B.D. Cullity and S.R. Stock, *Elements of X-ray Diffraction* (Upper Saddle River: Prentice Hall, 2011).
25. R. Yogamalar, R. Srinivasan, A. Vinu, K. Ariga, and A.C. Bose, *Solid State Commun.* 149, 1919 (2009).
26. A.K. Zak, W.H.A. Majid, M.E. Abrishami, and R. Yousefi, *Solid State Sci.* 13, 251256 (2011).
27. A. Zak, W. Majid, M. Abrishami, and R. Yousefi, *Solid State Sci.* 13, 251 (2011).

28. M. Birkholz, *J. Appl. Cryst*. 143 (2006).
29. T.M. Hammad, *Phys. Status Solidi A* 206, 2128 (2009).
30. G. Haacke, *J. Appl. Phys.* 47, 4086 (1976).
31. D.B. Fraser and H.D. Cook, *J. Electrochem. Soc.* 119, 1368 (1972).
32. K.N. Tonny, R. Rafique, A. Sharmin, M. Bashar, and Z. Mahmood, *AIP Adv.* 8, 065307 (2018).

Publisher's Note Springer Nature remains neutral with regard to jurisdictional claims in published maps and institutional affiliations.